Intersubband scattering in *n*-GaAs/AlGaAs wide quantum wells

I. L. Drichko,[1] I. Yu. Smirnov,[1] M. O. Nestoklon,[1] A. V. Suslov,[2] D. Kamburov,[3] K. W. Baldwin,[3] L. N. Pfeiffer,[3] K. W. West,[3] and L. E. Golub[1]

[1]*Ioffe Institute, 194021 St. Petersburg, Russia*

[2]*National High Magnetic Field Laboratory, Tallahassee, Florida 32310, USA*

[3]*Department of Electrical Engineering, Princeton University, Princeton, New Jersey 08544, USA*

(Received 12 January 2018; published 20 February 2018)

Slow magneto-oscilations of the conductivity are observed in a 75-nm-wide quantum well at heating of the two-dimensional electrons by a high-intensity surface acoustic wave. These magneto-oscillations are caused by intersubband elastic scattering between the symmetric and asymmetric subbands formed due to an electrostatic barrier in the center of the quantum well. The tunneling splitting between these subbands as well as the intersubband scattering rate are determined.

DOI: 10.1103/PhysRevB.97.075427

I. INTRODUCTION

Quantum structures with more than one occupied levels of size quantization represent an intermediate case between ultraquantum and bulk systems. A presence of a few two-dimensional subbands allows us to study interactions between electronic states of different types. An interesting example is intersubband scattering by a disorder potential. The typical systems with a few levels are quantum wells with two or more subbands under the Fermi level and double quantum wells. There is also another type of structure, called doped wide quantum wells (WQWs). They represent a bilayer system because the Coulomb repulsion results in a potential barrier in the middle of the WQW pushing the carriers towards the interfaces [1]. If these two layers are independent, then they act in transport as two parallel conducting channels. These two channels are identical with equal Fermi energies and relaxation times, provided the WQW is perfectly symmetric. In contrast, when tunneling through the potential barrier is not negligible, these two channels interact to each other, and the system's eigenstates are the symmetric (S) and antisymmetric (AS) states with the tunneling energy gap Δ_{SAS}. This gap has been studied in a variety of WQWs, for a review see Ref. [2]. Usually Δ_{SAS} is determined from the Fourier analysis of the magnetoresistance in the region of weak magnetic fields $B < 0.5$ T.

The presence of two channels results in a rich picture of conductivity oscillations in quantizing magnetic fields. In addition to the usual Shubnikov–de Haas effect, the other type of magneto-oscillations periodic in $1/B$ takes place. These oscillations are caused by elastic scattering between the S and AS subbands, the so-called magneto-inter-subband oscillations (MISO). They appear at $\Delta_{SAS}/\hbar\omega_c = K$, where ω_c is the cyclotron frequency and K is an integer number. Since this condition does not contain the Fermi energy, MISO are not damped by the Fermi distribution smearing. Therefore, in contrast to the Shubnikov–de Haas oscillations, MISO amplitude is almost insensitive to the temperature increase. MISO are well studied in various systems with two or three occupied subbands; for a review see Ref. [3] and references therein. Recently, a temperature dependence of MISO amplitude in a quantum well with three populated subbands has been explained by temperature variation of quantum electron lifetime [4], an energy spectrum reconstruction by a parallel magnetic field has been shown to affect MISO strongly [5,6], and the thermoelectric power magnetophonon resonance has been studied in two-subband quantum wells [7].

MISO are possible to observe only if they are not superimposed on the Shubnikov–de Haas oscillations. However both types of oscillations are present in the same magnetic field range in high-mobility WQWs. The Shubnikov–de Haas oscillations can be damped by increase of temperature. However, heating of the sample in the dc regime also results in an increase of the lattice temperature. This leads to an enhancement of electron scattering by phonons which damps MISO as well. Therefore MISO in high-mobility WQWs have not been observed so far.

We used acoustic methods with a surface acoustic wave (SAW) of high intensity applied in the pulsed regime with the duty factor equal to 100. This allowed heating of the electron system up to $T > 500$ mK while the lattice temperature was kept at 20 mK. As a result, the Shubnikov–de Haas oscillations were damped, and clear MISO were observed. We analyzed MISO in WQWs and determined the energy gap Δ_{SAS} and the intersubband scattering rate. We show that the theory of magneto-oscillations describes well the experimental data.

II. EXPERIMENT

The high-quality samples were multilayer n-GaAlAs/GaAs/GaAlAs structures with a 75-nm-wide quantum well. The quantum GaAs well was δ doped on both sides and located at the depth ≈197 nm below the surface of the sample. A structure of this type is known to be very symmetric, see, e.g., Ref. [8]. While cooling the sample down to 15 K and illuminating it with infrared light of emitting diode, we achieved the electron density of 1.4×10^{11} cm^{-2} and the mobility of 2.4×10^7 cm^2/(Vs) (at $T = 0.3$ K).

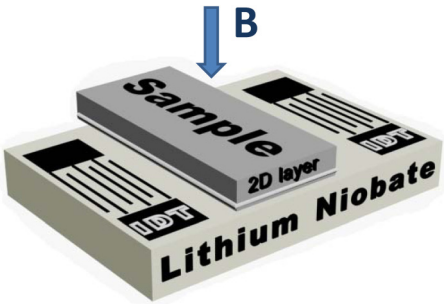

FIG. 1. Sketch of the experimental setup.

In the present paper we employ a SAW technique [9,10] illustrated in Fig. 1. A sample is pressed by means of springs to the surface of a piezoelectric crystal of lithium niobate ($LiNbO_3$), on which the interdigitated transducers (IDT) are formed. A radiofrequency electrical pulse signal is applied to one of the IDTs. Due to the piezoelectric effect, a SAW is generated and propagates along the surface of $LiNbO_3$. Simultaneously, an ac electric field, accompanying the SAW and having the same frequency, penetrates the sample and interacts with the charge carriers. This interaction results in a change of the SAW amplitude and in its velocity. The measurements were carried out in a dilution refrigerator in a magnetic field perpendicular to the sample plane.

The dependencies of the attenuation $\Gamma(B)$ and the relative velocity change $\Delta v(B)/v_0$ of the surface acoustic wave were measured in a magnetic field of up to 1 T in the temperature range 20–500 mK and the frequency range 28.5–300 MHz at different SAW intensities. Figure 2 shows the experimental dependencies of the SAW attenuation Γ and velocity shift $\Delta v/v_0$ at the frequency 30 MHz, measured at the temperature $T \approx 20$ mK with the SAW power introduced into the sample of 1.2×10^{-6} W/cm. During the measurements, the magnetic field was swept from -1 to 1 T (red curve) and then went back to -1 T (blue curve) ramping as 0.05 T/min. The curves of these forward and reverse field sweeps are almost identical. A Hall probe was used to measure the magnetic field strength.

The SAW attenuation and the velocity change are governed by the complex ac conductance $\sigma(\omega) \equiv \sigma_1(\omega) - i\sigma_2(\omega)$. Both the real σ_1 and imaginary σ_2 components of $\sigma(\omega)$ could be extracted from our acoustic measurements. The procedure of the determination of the ac conductance is described in Ref. [10] and is based on using that work Eqs. (1)–(7).

The dependencies of the real part σ_1 of the high-frequency conductance, calculated from the SAW attenuation and velocity change, on the reversed magnetic field $1/B$ measured at various temperatures from 20 to 510 mK are presented in Fig. 3(a). The dependencies $\sigma_1(1/B)$ recorded at several SAW intensities are plotted in Fig. 3(b), where effective SAW power introduced into the sample ranged from 3.7×10^{-10} W/cm to 3.7×10^{-5} W/cm.

As seen in Fig. 3, the Shubnikov—de Haas oscillations are observed at low SAW intensities. These fast oscillations have the period determined by the Fermi energies in the subbands. Since the Fermi energies have slightly different

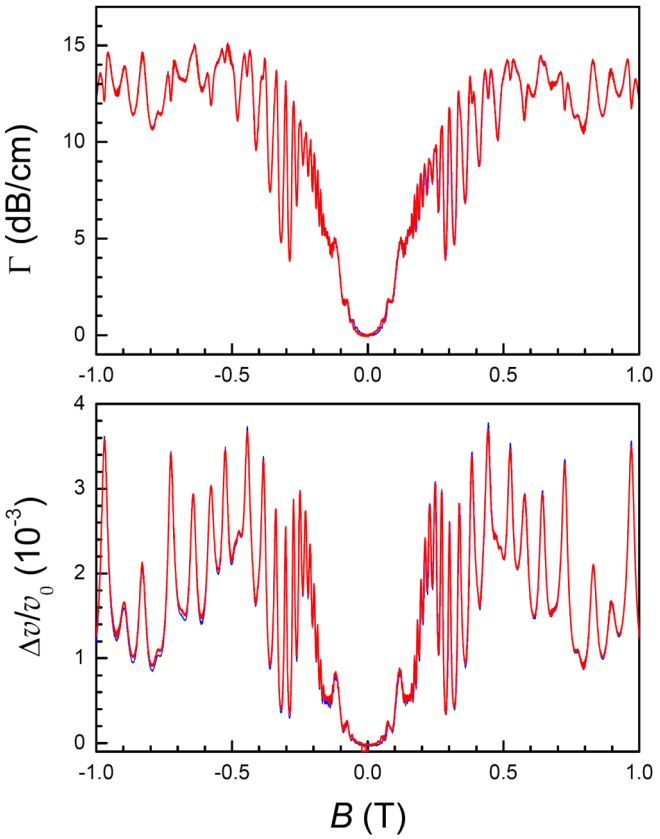

FIG. 2. Dependencies of the SAW attenuation coefficient Γ (top panel) and the SAW velocity change $\Delta v(B)/v_0$ (bottom panel) on the transverse magnetic field B at $f = 30$ MHz, $T = 20$ mK; SAW power introduced into the sample is 1.2×10^{-6} W/cm. Red and blue curves (almost identical) show forward and reverse field sweeps.

values $E_F \pm \Delta/2$, the independent oscillating contributions to the conductivity from the subbands undergo a beating. At high temperatures their amplitudes decrease. Moderate increasing of the SAW power affects the real part of ac conductance σ_1 in the same way as the temperature rising does, see Fig. 3(b). However, with further growth of the SAW power, these fast oscillations virtually vanish, and the slow oscillations emerge. The latter dominates at the highest SAW intensities. The positions of the slow oscillations minima are independent of the SAW frequency. We assume that the slow oscillations are not distinguishable in Fig. 3(a) due to the small signal-to-noise ratio in the low-power regime used when we acquired the curves presented in this figure.

The structure of the fast and slow oscillations is presented in more detail in Fig. 4. Here the dependence of $\sigma_1(B)$ is shown for $f = 30$ MHz at 20 mK, and the SAW power pushed into the sample was 1.2×10^{-6} W/cm. This picture demonstrates the SdH oscillations marked with filling factors ν. In lower fields $B < 0.4$ T, one can observe a new series of oscillations denoted by letter K.

III. DISCUSSION

From the analysis of the slope of the dependence $\nu(1/B)$ shown in Fig. 4(b) we determined the Fermi energy in the

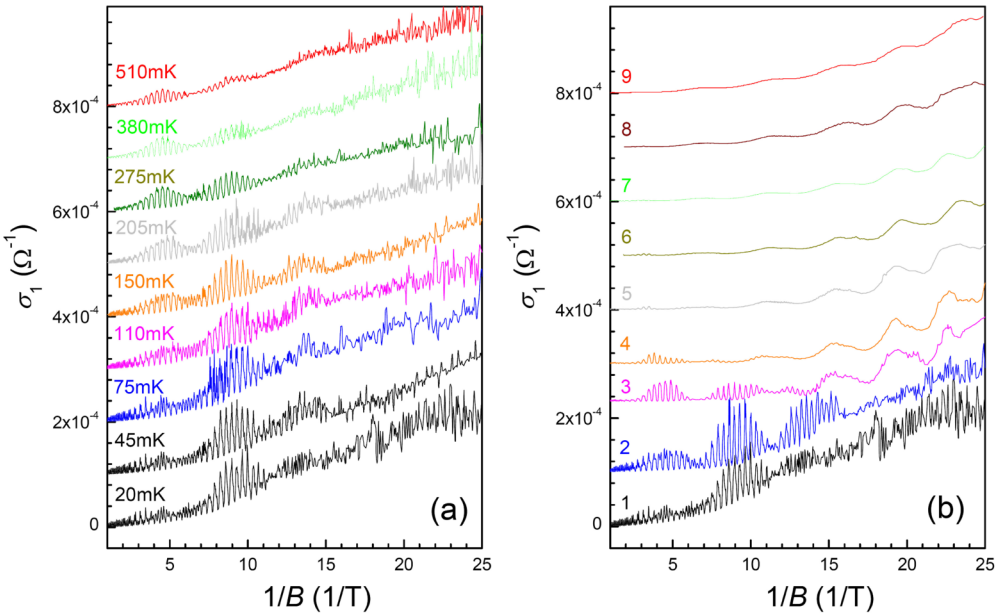

FIG. 3. (a) Dependencies of σ_1 on the inverse magnetic field as varied with temperature at the SAW power introduced into the sample of 3.7×10^{-10} W/cm and (b) as varied with the SAW powers at $T = 20$ mK: 1–3.7×10^{-10} W/cm, 2–1.2×10^{-8} W/cm, 3–1.3×10^{-7} W/cm, 4–3.6×10^{-7} W/cm, 5–1.2×10^{-6} W/cm, 6–2.3×10^{-6} W/cm, 7–5.9×10^{-6} W/cm, 8–1.2×10^{-5} W/cm, and 9–3.7×10^{-5} W/cm; $f = 30$ MHz. Traces are offset vertically for clarity.

studied WQW as $E_F \approx 2.5$ meV. The slow oscillations demonstrate a presence of an energy gap $\Delta \ll E_F$ in the electronic spectrum. We extracted this splitting from the dependence $K(1/B)$ drawn in Fig. 4(a): $\Delta = 0.42 \pm 0.02$ meV.

In order to explain an origin of this energy splitting, we performed self-consistent calculations of the electrostatic potential and electron wave functions. First, the wave functions are calculated in the tight-binding approach [11]. Then, the electron wave functions are used to calculate the electron density distribution in the quantum well

$$n(z) = \sum_{i,s} \int d\boldsymbol{k}_\parallel \, f_0(E_{i,s}(\boldsymbol{k}_\parallel) - E_F)|\psi_{i,s}(z;\boldsymbol{k}_\parallel)|^2, \qquad (1)$$

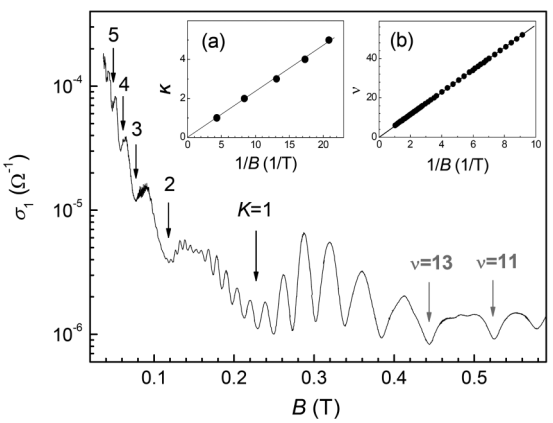

FIG. 4. Magnetic field dependence of σ_1 at $f = 30$ MHz and $T \approx 20$ mK. The SAW power introduced into the sample is 1.2×10^{-6} W/cm. (a) Dependence of the slow oscillations number K on $1/B$. (b) Dependence of the filling factors ν on $1/B$.

where $\psi_{i,\uparrow(\downarrow)}(z;\boldsymbol{k}_\parallel)$ and $E_{i,\uparrow(\downarrow)}(\boldsymbol{k}_\parallel)$ are the wave function and energy of a spin up(down) electron at ith quantum confined level with lateral wave vector $\boldsymbol{k}_\parallel$, and the Fermi-Dirac distribution function $f_0(\epsilon) = [1 + \exp(\epsilon/k_BT)]^{-1}$ gives the population of the levels. Neglecting the nonparabolicity of the electron dispersion which is small in AlGaAs-based systems, we obtain the wave functions independent of the wave vector, and Eq. (1) simplifies to

$$n(z) = \sum_{i,s} n_{i,s}|\psi_{i,s}(z)|^2 , \qquad (2)$$

where $n_{i,s} = \int_{\boldsymbol{k}_\parallel} f_0(E_{i,s}(\boldsymbol{k}_\parallel) - E_F)$.

In the studied structure, the Fermi level lies between the second and third levels provided the temperature is small compared with the Fermi energy $k_BT \ll E_F$. Moreover, as the energy splittings of the levels, Δ, are also small compared to E_F, the total electron density is equally distributed between those levels, and we have

$$n(z) = \frac{n_{\text{total}}}{4} \sum_{i=1,2;\,s} |\psi_{i,s}(z)|^2 . \qquad (3)$$

We have numerically checked that taking into account a nonequality $n_1 \neq n_2$, the values of the splittings are not changed within the calculation accuracy. The value of the total electron density extracted from our experiment is $n_{\text{total}} = 1.4 \times 10^{11}\text{cm}^{-2}$. To compensate the charge inside the WQW and make the structure uncharged, we assumed that the charge $-n_{\text{total}}/2$ is uniformly distributed in the barriers starting from the position where the distribution of electron density $n(z)/n_{\text{total}}$ drops below 10^{-4}. The electrostatic potential corresponding to the charged QW is found from the numerical

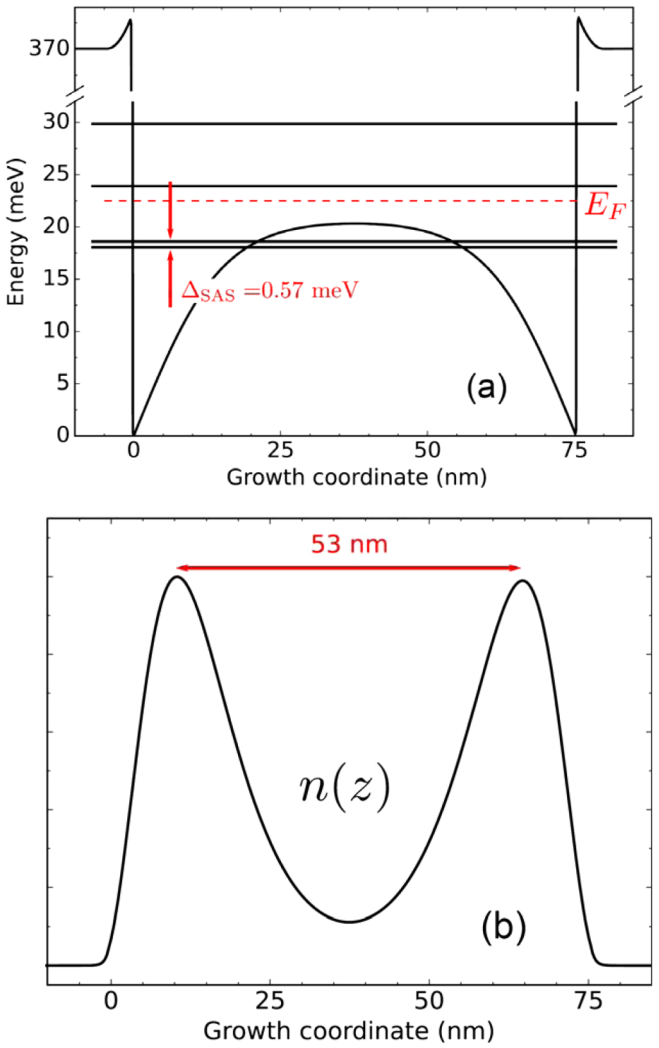

FIG. 5. Self-consistently calculated energy levels and the heteropotential (a) and the electron density profile (b).

solution of Poisson equation

$$\phi''(z) = -\frac{4\pi e}{\varepsilon} n(z), \tag{4}$$

with the dielectric constant $\varepsilon = 12.9$. Then, we add $\phi(z)$ to the structure potential and compute the next approximation for the electron wave functions of the levels in the WQW. The procedure is repeated until the self-consistency of the electron wave functions and electrostatic potential is reached.

The results for the converged potential and the electron density distribution are presented in Fig. 5. The position of the first two levels is close to the local maximum of the heteropotential, Fig. 5(a). This fact makes a convergence of the calculation scheme slow for our quantum well width and concentration. The electron density profiles shown in Fig. 5(b) for the two first levels, $|\psi_{1,s}(z)|^2 \approx |\psi_{2,s}(z)|^2$, almost coincide for all $s = \uparrow, \downarrow$. The distance 53 nm between the density profile maxima agrees with the value for WQWs of the same width [2,12]. The calculated S-AS splitting $\Delta_{SAS} = 0.57$ meV.

In the triangular quantum wells formed near the structure edges, Fig. 5(a), the spin-orbit splitting is present which can give rise to the beating pattern in magneto-oscillations [13,14]. Our tight-binding method allows us also to estimate the spin splittings of the two first subbands caused by the quantum confinement and electric field in the structure [15]. The calculations show that the spin-orbit splitting of the electronic states at the Fermi wave vector is $\Delta_{so} \approx 0.01$ meV in the WQW under study. Since $\Delta_{so} \ll \Delta_{SAS}$, we conclude that the spin-orbit splitting is negligible at such a low carrier density.

The calculated S-AS energy splitting $\Delta_{SAS} = 0.57$ meV is close to the value $\Delta \approx 0.42$ meV determined from the experiment. Therefore we conclude that it is the intersubband scattering that results in slow magneto-oscillations of the heated electron gas in the WQW under study.

The conductivity magneto-oscillations with account for both S-AS splitting and scattering between S and AS subbands are described by the following expression [3,16]:

$$\sigma_{xx} = \frac{\sigma_0}{(\omega_c\tau)^2}\left[1 - 4\cos\left(2\pi\frac{E_F}{\hbar\omega_c}\right)\cos\left(\pi\frac{\Delta_{SAS}}{\hbar\omega_c}\right) \times e^{-\pi/\omega_c\tau_q}\frac{X}{\sinh X} + 2\frac{\tau}{\tau_{SAS}}\cos\left(2\pi\frac{\Delta_{SAS}}{\hbar\omega_c}\right)e^{-2\pi/\omega_c\tau_q}\right]. \tag{5}$$

Here σ_0 is the conductivity at zero magnetic field, τ is the transport scattering time which determines the mobility, τ_q is the quantum scattering time, ω_c is the cyclotron frequency, and $X = 2\pi^2 k_B T/\hbar\omega_c$. The time τ_{SAS} is the time of elastic scattering between the S and AS subbands. This expression is valid in moderate magnetic fields where $e^{-\pi/\omega_c\tau_q} \ll 1$ but $\omega_c\tau \gg 1$, and at weak intersubband scattering, $\tau/\tau_{SAS} \ll 1$. The first oscillating term in Eq. (5) describes the beating pattern in the Shubnikov–de Haas oscillations in the two-subband system with close Fermi energies $E_F \pm \Delta_{SAS}/2$. These beatings are damped by heating of the electron gas due to smearing of the Fermi distribution as described by the factor $X/\sinh X$. In contrast, the second oscillating term caused by MISO, being inferior at low temperatures, dominates at high temperatures when $X/\sinh X \ll e^{-\pi/\omega_c\tau_q}$ [17,18]. Equation (5) indicates that the beating frequency is 2 times smaller than that for the slow oscillations. Indeed, this is observed in our experiment, Fig. 3.

We estimated an intensity of intersubband scattering from the amplitude of MISO. Analysis of the data at the SAW powers 1.2×10^{-6} W/cm and 1.3×10^{-7} W/cm with help of Eq. (5) yields $\tau/\tau_{SAS} = 0.35 \pm 0.05$ and $\tau_q = 4 \times 10^{-11}$ s. The value of τ_q agrees with the quantum scattering time determined for similar WQWs [4]. The transport scattering time is known from mobility: $\tau = 0.9 \times 10^{-9}$ s at 0.3 K. This yields $\tau_{SAS} = 2.6 \times 10^{-9}$ s. The intersubband scattering time 3 times longer than the transport scattering time means that the intersubband scattering in the studied WQW is weaker than the intra-subband scattering but it is strong enough for observation of MISO.

IV. CONCLUSION

To conclude, we observed the magneto-inter-subband oscillations of the conductivity in a WQW. The oscillations are shown to arise due to elastic intersubband scattering between the S and AS subbands formed due to Coulomb

repulsion between the electrons. A tight-binding calculation of the electron states yields the splitting Δ_{SAS} close to the experimentally measured value. Our theoretical description of the magneto-oscillations allowed to determine the quantum and the intersubband scattering times.

ACKNOWLEDGMENTS

The authors thank L. Yu. Shchurova for help in calculations, Yu. M. Galperin for discussions, and E. Palm, T. Murphy, J.-H. Park, and G. Jones for technical assistance. Partial support from Presidium of RAS and the Russian Foundation for Basic Research (Project No. 16-02-0037517) is gratefully acknowledged. L.E.G. thanks "BASIS" foundation. The National High Magnetic Field Laboratory is supported by National Science Foundation Cooperative Agreement No. DMR-1157490 and the State of Florida. The work at Princeton was supported by the Gordon and Betty Moore Foundation through EPiQS initiative Grant No. GBMF4420 and by NSF MRSEC Grant No. DMR-1420541.

[1] Y. W. Suen, J. Jo, M. B. Santos, L. W. Engel, S. W. Hwang, and M. Shayegan, Missing integral quantum Hall effect in a wide single quantum well, Phys. Rev. B **44**, 5947(R) (1991).

[2] M. Shayegan, H. C. Manoharan, Y. W. Suen, T. S. Lay, and M. B. Santos, Correlated bilayer electron states, Semicond. Sci. Technol. **11**, 1539 (1996).

[3] I. A. Dmitriev, A. D. Mirlin, D. G. Polyakov, and M. A. Zudov, Nonequilibrium phenomena in high Landau levels, Rev. Mod. Phys. **84**, 1709 (2012).

[4] S. Dietrich, J. Kanter, W. Mayer, S. Vitkalov, D. V. Dmitriev, and A. A. Bykov, Quantum electron lifetime in GaAs quantum wells with three populated subbands, Phys. Rev. B **92**, 155411 (2015).

[5] W. Mayer, J. Kanter, J. Shabani, S. Vitkalov, A. K. Bakarov, and A. A. Bykov, Magnetointersubband resistance oscillations in GaAs quantum wells placed in a tilted magnetic field, Phys. Rev. B **93**, 115309 (2016).

[6] W. Mayer, S. Vitkalov, and A. A. Bykov, Resistance oscillations of two-dimensional electrons in crossed electric and tilted magnetic fields, Phys. Rev. B **93**, 245436 (2016).

[7] A. D. Levin, G. M. Gusev, O. E. Raichev, and A. K. Bakarov, Magnetophonon oscillations of thermoelectric power and combined resonance in two-subband electron systems, Phys. Rev. B **94**, 115309 (2016).

[8] M. Shayegan, Flatland electrons in high magnetic fields, in *High Magnetic Fields: Science and Technology*, edited by F. Herlach and N. Miura, Vol. 3 (World Scientific, Singapore, 2006), p. 31.

[9] A. Wixforth, J. Scriba, M. Wassermeier, J. P. Kotthaus, G. Weimann, and W. Schlapp, Surface acoustic waves on GaAs/Al_xGa_{1-x}As heterostructures, Phys. Rev. B **40**, 7874 (1989).

[10] I. L. Drichko, A. M. Diakonov, I. Yu. Smirnov, Y. M. Galperin, and A. I. Toropov, High-frequency hopping conductivity in the quantum Hall effect regime: Acoustical studies, Phys. Rev. B **62**, 7470 (2000).

[11] J.-M. Jancu, R. Scholz, F. Beltram, and F. Bassani, Empirical spds* tight-binding calculation for cubic semiconductors: General method and material parameters, Phys. Rev. B **57**, 6493 (1998).

[12] L. Shchurova and Y. M. Galperin, Electron concentration profiles in modulation doped structures with wide quantum well, Phys. Status Solidi C **14**, 1700190 (2017).

[13] Yu. A. Bychkov and É. I. Rashba, Oscillatory effects and the magnetic susceptibility of carriers in inversion layers, J. Phys. C: Solid State Phys. **17**, 6039 (1984).

[14] P. Ramvall, B. Kowalski, and P. Omling, Zero-magnetic-field spin splittings in $Al_xGa_{1-x}As$/GaAs heterojunctions, Phys. Rev. B **55**, 7160 (1997).

[15] P. S. Alekseev and M. O. Nestoklon, Effective one-band approach for the spin splittings in quantum wells, Phys. Rev. B **95**, 125303 (2017).

[16] O. E. Raichev, Magnetic oscillations of resistivity and absorption of radiation in quantum wells with two populated subbands, Phys. Rev. B **78**, 125304 (2008).

[17] N. S. Averkiev, L. E. Golub, S. A. Tarasenko, and M. Willander, Theory of magneto-oscillation effects in quasi-two-dimensional semiconductor structures, J. Phys.: Condens. Matter **13**, 2517 (2001).

[18] N. C. Mamani, G. M. Gusev, T. E. Lamas, A. K. Bakarov, and O. E. Raichev, Resonance oscillations of magnetoresistance in double quantum wells, Phys. Rev. B **77**, 205327 (2008).